THE AMERICAN SOCIETY OF MECHANICAL ENGINEERS
Three Park Avenue, New York, N.Y. 10016-5990

99-GT-161

Formation of Counter-Rotating Vortices in Film-Cooling Flows

C. A. Lemmon, A. Kohli* and K. A. Thole
Mechanical Engineering Department
University of Wisconsin
Madison, Wisconsin 53706

Abstract

Film-cooling is a widely used method of cooling turbine airfoils in high performance gas turbine engines. A typical hole geometry is a short, round hole that is inclined at 35° with respect to the external surface. One characteristic of this film-cooling flowfield is the formation of a counter-rotating vortex pair downstream of the jet injection. This vortex pair is located downstream of injection and has been documented by both experimental and computational studies. There are a number of studies in the literature that suggest that this vortex pair originates from the vorticity in the boundary layers of the cooling hole.

This paper addresses the formation mechanism of the counter-rotating vortex pair: is it generated by the vorticity inside the film-cooling hole or the jet-mainstream interaction? To answer this question, two different computational cases were compared. One case is a viscous solution with a no-slip boundary condition applied on all walls. The other is a viscous solution with slip boundary conditions imposed on all walls. This study considers a jet-to-mainstream density ratio of two and a mass flux ratio of a half. The results of this computational experiment indicate that the counter-rotating vortices exist in both cases. This suggests that the vortex generation mechanism is the interaction between the jet and the mainstream.

Introduction

In many gas turbine engine designs, turbine airfoils are cooled using air that has been extracted from the compressor. This bleed air is directed into the turbine airfoils to convectively cool the inside surface and the discrete film-cooling passages placed in the blade surface. After the cooling air exits from the holes, the fluid provides film-cooling on the outside surface.

A typical film-cooling hole geometry is a round hole that is inclined by 35° with respect to the mainstream flow. The cooling hole length-to-diameter ratio can vary, but typical ranges are between $1 < L/D < 6$. Over the years, experimental and computational studies have identified key characteristics of film-cooling flows. One characteristic is the counter-rotating vortex pair formed downstream of injection. These counter-rotating vortices move hot gas underneath the film-cooling jet, thereby reducing the cooling effectiveness as the flow progresses downstream. Subsequently, there is an interest in determining the mechanism that forms these counter-rotating vortices.

This paper presents an analysis whereby a numerical experiment was performed using computational fluid dynamics (CFD) to determine the source of the counter-rotating vortices. Specifically this study was designed to answer the question: are the counter-rotating vortices formed downstream of jet injection due to the jet-mainstream interaction or due to the vortical nature of the flow inside the cooling hole? The vortical nature of the flow inside the cooling hole is a result of two different phenomena. One phenomenon is the vorticity contained within the hole boundary layers. The other phenomenon is the counter-rotating vortices formed inside the cooling hole as a result of the flow turning at the entrance of the hole.

Two different cases will be compared to determine the formation mechanism. The first case is the realistic viscous solution with no-slip boundary conditions, which has been previously published by a number of investigators through both CFD and experiments. The supply to the cooling hole is through a stagnant plenum. The second case is also a viscous solution, but instead of using a no-slip boundary condition, a slip boundary condition is imposed for all of the surfaces. A slip condition at the walls results in no boundary layer formation inside the cooling hole or in the mainstream. Although the slip condition is not realistic, it will help to isolate the source of the vortex pair. Also for this second case, a constant velocity profile is specified at the hole inlet. This removes any turning of the flow at the hole entrance.

The geometry used for this study is a round film-cooling hole that is inclined at 35° with an $L/D = 4$. The density ratio was $DR = 2$ and the mass flux ratio was $M = 0.5$. These result in a relatively low velocity ratio of $VR = 0.25$.

The following sections discuss past relevant studies, the CFD method used in this study and some benchmark results, present results of the computational experiments, and finally some conclusions.

* Present address is Pratt & Whitney, 400 Main Street, MS 169-02, East Hartford, CT 06108

Presented at the International Gas Turbine & Aeroengine Congress & Exhibition
Indianapolis, Indiana — June 7–June 10, 1999

Past Studies

Andreopoulos and Rodi (1984) identified counter-rotating vortices with their normal jet injection studies with a relatively long hole length of L/D = 12. They stated that the generation of the vorticity at small velocity ratios (VR < 0.5) is primarily due to the re-orientation of the vorticity formed inside the jet hole, with a small contribution due to the shear at the jet-cross-flow interface. At higher velocity ratios, the generation of the counter-rotating vortices is primarily due to the interfacial shear between the cross-flow and jet.

For film-cooling applications, the jet is typically shorter in length and inclined at 30° - 35° with respect to the mainstream direction. Pietrzyk (1989) was the first to present flowfield measurements showing that kidney-shaped, counter-rotating vortices exist for an inclined jet. Pietrzyk, et al. (1989) also postulated that a separation region occurred at the entrance on the leeward side of the film-cooling hole causing high turbulence and a skewed velocity profile at the hole exit. The computational study presented by Leylek and Zerkle (1994), which simulated the study of Pietrzyk, et al. (1989), also showed the counter-rotating vortices downstream of injection, but in addition showed counter-rotating vortices inside the cooling hole. The vortices inside the hole have the same sense of rotation as the vortices downstream of the jet injection.

There is evidence in the literature that disagrees with the idea that the counter-rotating vortices downstream of jet injection are due to the counter-rotating vortices generated inside the cooling hole. Kohli and Thole (1997) performed computations for a jet supplied by a plenum, as was the condition for the cases discussed above, and for a jet supplied by a perpendicular cross-flow at the hole entrance. The velocity vectors inside the hole indicated two different vortical patterns. For the plenum case, as discussed previously, the counter-rotating vortex motion occurred due to the flow turning over the separation region present on the leeward side of the hole. For the perpendicular cross-flow case, a single swirling vortex developed inside the hole. Although the vortex structures inside the hole were different for the two cases, counter-rotating vortices formed downstream of injection for both cases. This supports the theory that the counter-rotating vortices downstream of injection are not simply the vortex formed inside the cooling hole. Haven, et al. (1997) and Vogel (1998) attribute the formation of these vortices to the interaction between the jets and the cross-flow rather than the vortex pattern inside the cooling hole.

Other investigators have suggested that the counter-rotating vortices formed downstream of the hole are a result of the boundary layer vorticity inside the cooling hole. Sgarzi and Leboeuf (1997), for example, state that the origin of the counter-rotating vortices are connected with the vortex rings of the boundary layer fluid exiting the hole. Walters and Leylek (1997) point out that the two sources causing the counter-rotating vortices are the shear from the jet-mainstream interaction and the vorticity inside the cooling hole, with the latter being more relevant. They state several reasons why the interfacial shear is not significant, with one reason being that the jet is inclined thereby not bending as much as a normal jet.

Coelho and Hunt (1989) performed an analysis using a three-dimensional, inviscid vortex sheet model of strong jets in cross-flows. The solution indicated that additional axial and transverse vorticity within the pipe was generated due to pressure gradients imposed by the external flow. As the flow approaches the hole exit, tangential pressure gradients along the hole walls generate vorticity. Given that this is an inviscid approach, it supports the idea that the boundary layer inside the hole does not need to be present to form the counter-rotating vortices.

Clearly, there is some disagreement as to the source of the counter-rotating vortices. By removing the counter-rotating vortices and the boundary layer inside the hole, it is possible to establish whether the counter-rotating vortices downstream still form. This would support the theory that the source of the vortex generation is the jet - mainstream interaction (Bogard, 1998).

Computational Domain and Geometry

The computational domain for the round cooling hole geometry, which consists of the mainstream flow, the film-cooling hole, and the plenum, is shown in Figure 1a. The flow conditions for this study were a mass flux ratio of M = 0.5 and a density ratio of DR = 2.

The streamwise extent of the computational domain was $-19 \le x/D \le 30$, which is similar to the domain used in past CFD studies by Berhe and Patankar (1996) and Walters and Leylek (1997). A uniform inlet velocity of U_∞ = 20 m/s was applied as a boundary condition at the inlet of the domain. An outflow boundary condition was applied at the exit of the domain since the gradients in the streamwise direction are expected to be small at x/D = 30. In the vertical direction, the computational domain extends out to y/D = 10, which is sufficiently far from the film-cooling flowfield to allow a zero gradient boundary condition to be imposed. A symmetry condition is applied on both the jet centerline and the half-pitch line. The spanwise extent of the computational domain was $-1.5 < z/D < 0$.

For both cases in this study, adiabatic boundary conditions were applied on all wall surfaces for the energy equation. For the viscous, no-slip case, a plenum supplied the cooling hole. The plenum had a height of H/D = 3, and it extended 5D upstream and 5D downstream of the en-

Nomenclature

D = hole diameter
DR = density ratio defined as $DR = \rho_j/\rho_\infty$
H = height of plenum
k = turbulent kinetic energy
L = length of film cooling hole
M = blowing ratio defined as $M = \rho_j U_j/\rho_\infty U_\infty$
T = temperature
U_∞ = freestream velocity
U_j = jet velocity
u_τ = wall velocity, defined as $\sqrt{(\tau w/\rho)}$
V = velocity magnitude
VR = velocity ratio defined as $VR = U_j/U_\infty$
x = streamwise direction measured from hole centerline, see Figure 1a
y = vertical direction, see Figure 1a
y^+ = $y u\tau/\nu$
z = spanwise direction from hole center

Greek

ε = turbulent dissipation rate
ρ = density
η = adiabatic effectiveness, defined as $\eta = (T_\infty - T_\infty) / (T_j - T_\infty)$
θ = momentum thickness
Θ = normalized temperature, defined as $\Theta = (T - T_\infty) / (T_j - T_\infty)$
Ω = vorticity magnitude
Ω^* = normalized vorticity magnitude, WD/U_∞
τ_∞ = wall shear stress
ν = kinematic viscosity

Subscripts

aw = adiabatic wall
∞ = freestream
j = jet

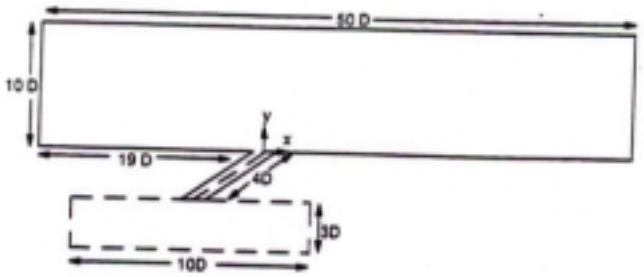

Fig. 1a Schematic of the computational domain.

trance to the film-cooling hole. An inlet velocity boundary condition was imposed at the bottom face of the entire plenum length. The momentum Reynolds number at two diameters upstream of the jet injection for the viscous case was $Re_e = 1075$. For the slip wall case, the plenum was removed from the domain, and all of the walls were considered to have a slip boundary condition. A constant velocity profile was applied at the entrance to the cooling hole as the inlet boundary condition. This boundary condition was used to ensure that the jet turning and separation region at the hole entrance did not exist; therefore, no counter-rotating vortices developed inside the cooling hole.

These CFD simulations were completed with a software package by Fluent, Inc., similar to that used by Walters and Leylek (1997), and Kohli and Thole (1997). An unstructured mesh was used for these studies. Grid adaptions were based on the gradients of flow variables of the solutions and on domain boundaries to achieve grid independent results. The unstructured mesh for the slip wall condition is shown in Figure 1b at the film-cooling hole centerline. The unstructured mesh for the no-slip wall case is shown in Figure 1c at a vertical plane through the center of the hole. Second-order discretization was used for the governing equations for momentum, energy, and turbulence. Turbulence closure was achieved by using the standard k-ε model (Launder and Spalding, 1974) with non-equilibrium wall functions (Kim and Choudhury, 1995). Fluent/UNS solves the RANS equations with a pressure based finite-volume scheme. The SIMPLE algorithm was used to solve the discretized equations with multi-grid acceleration.

Fig. 1b The unstructured grid used for the slip wall case.

The average cell skewness for the tetrahedral, unstructured grid for the no-slip case was 0.42. The cells near the wall maintained an average height of $y^+ = 23$, which was required for proper usage of the wall function model. For the slip wall case, the average cell skewness was 0.36. The number of cells used was nominally 390,000 for the half-hole simulations. The solution initialization was done using the freestream velocity and temperature. Flow solutions were obtained using an under-relaxation parameter for momentum, k and ε of 0.8 for the slip wall and 0.2 for the no-slip wall. For each case, a solution to the momentum equation (with the cooling hole at the freestream temperature) was obtained before beginning the energy solution (with the supply channel temperature such that DR = 2).

To ensure that a grid independent solution was obtained, it was verified that further gradient adaption changed the value of laterally averaged effectiveness near the hole by less than $\Delta\eta = 0.005$. The total number of iterations required for convergence for each of the cases was about 1500 iterations. For these solutions, values of centerline and laterally averaged effectiveness near the hole changed by less than $\Delta\eta_{cl} = 0.001$ and $\Delta\eta = 0.0001$ respectively over an additional 1000 iterations. At the same time, values of the velocity magnitude near the film-cooling hole changed by less than $\Delta V = 0.003$ m/s. Figure 1d shows velocity vectors at a vertical plane 1D downstream of injection for the no-slip case with 235,000 cells; while Figure 1e shows the same plane with 390,000 cells. These figures show the grid independence of the solution.

Fig. 1c The unstructured grid for the no-slip wall case, shown at x/D = 0.

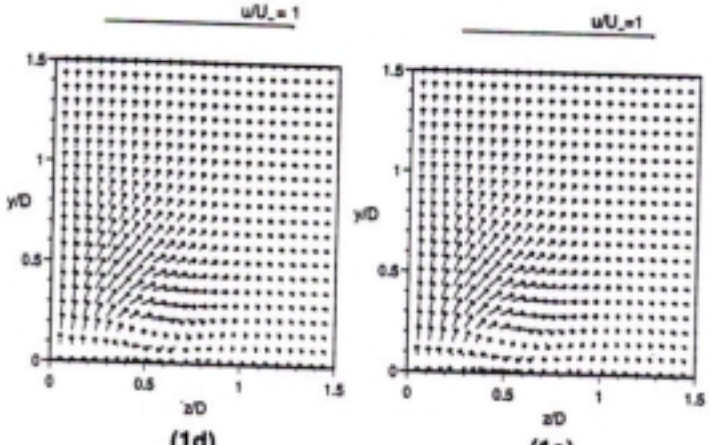

(1d) (1e)

Fig. 1d and 1e Velocity vectors at x/D = 1 for 230,000 cell (1d) and adapted 390,000 cell (1e) grids.

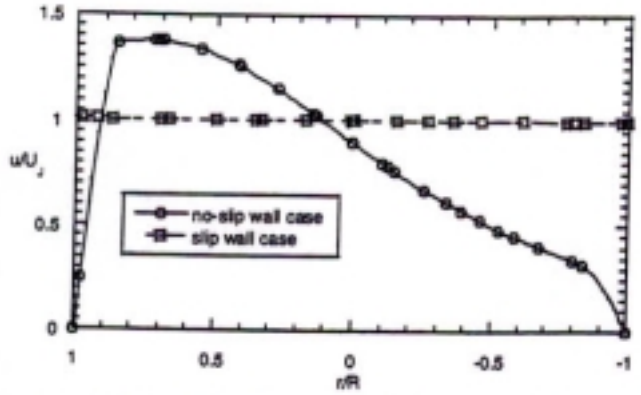

Fig. 2a Velocity profiles inside the film-cooling hole at two diameters downstream of the hole inlet for the no-slip and slip wall cases.

Results

In this section, results for the two different wall boundary conditions are compared with one another to determine its effect on the counter-rotating vortex and to try and discern the formative mechanism of these vortices. As most studies in literature have postulated that boundary layers (vorticity) generated inside the cooling hole lead to the formation of these vortices, it is important to discuss differences in the flowfield inside the cooling hole for the two cases.

Figure 2a shows the velocity profiles at a location that is half-way down the length of the cooling hole. It is clear that for the slip condition with the uniform inlet profile, the velocity is constant across the hole. For the no-slip condition, the velocity profile is skewed with higher velocities present towards the upstream side of the hole. This is caused by the flow jetting around the separation region which forms due to the flow turning through a large angle at the entrance to the cooling hole. This separation region is shown by the velocity vectors on the centerline of the jet for the no-slip boundary condition as presented in Figure 2b. (Note that the vectors were obtained for the unstructured grid results and interpolated on to a uniform grid.) Although not shown here, a counter-rotating vortex pair inside the film-cooling hole also formed. This is consistent with previous investigations (for example, Leylek and Zerkle, 1994). This counter-rotating vortex pair inside the cooling hole is formed because of the large turning angle experienced by the jet fluid at the hole entrance. The velocity vectors for the slip wall, shown in Figure 2c, indicate a uniform distribution across the hole. For the slip wall case with a uniform inlet velocity profile, no counter-rotating vortices are formed inside the cooling hole.

The differences in the velocity field, as seen in Figures 2b and 2c, occur primarily at the hole edges. On the upstream edge of the hole, there is a stronger penetration of the jet into the mainstream for the no-slip condition. This is because the cooling jet has higher velocities in that region of the hole. On the downstream edge of the hole, there is a stronger penetration of the jet into the mainstream for the slip wall since there is no boundary layer present inside the hole, as compared with the no-slip wall. Although a plot of vorticity inside the film-cooling hole is not shown here, the counter-rotating vortices inside the cooling hole do exist for the no-slip boundary condition case. There are no counter-rotating vortices inside the cooling hole for the slip wall case.

Figures 3, 6, and 8 show secondary velocity vectors and thermal field contours in planes that are perpendicular to the flow direction for the two cases at x/D = 0, 1, and 5. The thermal field contours are shown in increments of $\theta = 0.2$. The vectors and contours at x/D = 0, shown in Figure 3, correspond to a vertical-lateral slice at the center of the hole exit plane including the inside of the cooling hole. Note that the edge of the cooling hole is at z/D = 0.5. The secondary velocity vectors indicate that the vortex pair is already forming. The slip wall case shows a significantly stronger lateral motion of the jet fluid at the hole edge. The thermal contours show a cold core with very sharp gradients at the edges, which is an indication of the strong shear layer that exists between the jet and the mainstream flow. For the slip wall case, this shear layer is the only source of vorticity in the flow and will be discussed in detail later. The gradients are much sharper for the slip wall case, as indicated by the contour levels being closer together.

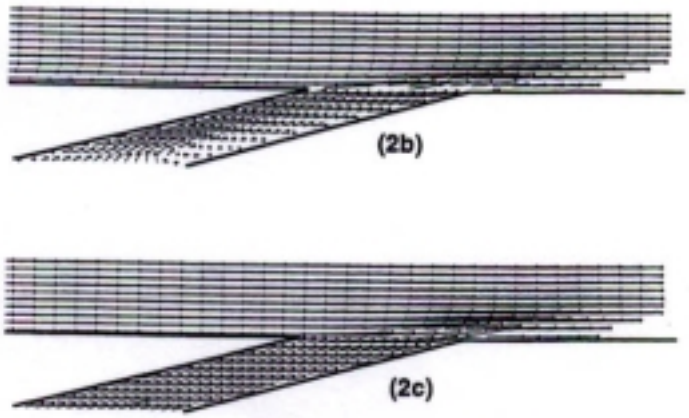

Fig. 2b and 2c Velocity vectors at the cooling hole centerline for the no-slip (2b) and slip (2c) walls.

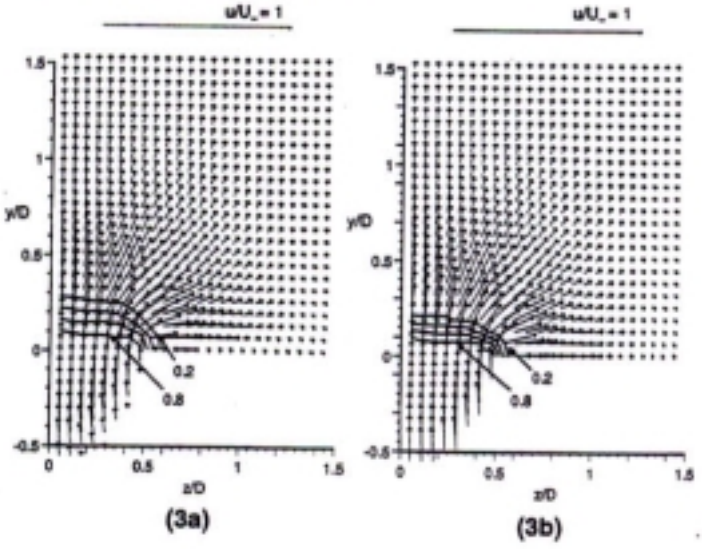

Fig. 3a and 3b Non-dimensional velocity vectors and thermal field contours (θ) at x/D = 0 for the no-slip (3a) and slip (3b) cases.

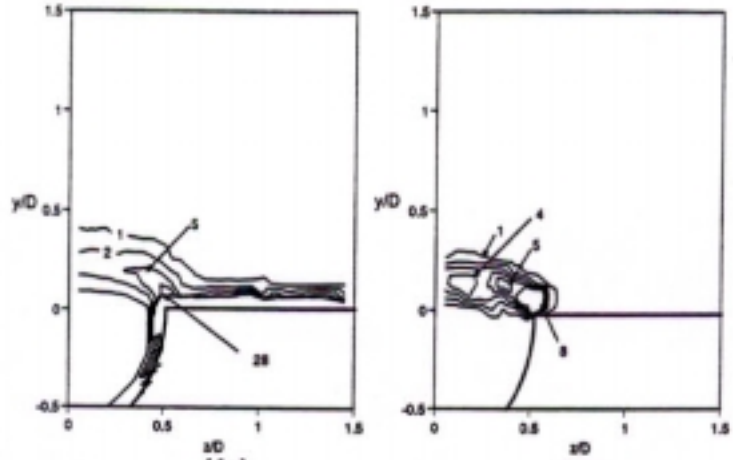

Fig. 4a and 4b Contours of normalized vorticity magnitude (Ω^*) at x/D = 0 for the no-slip (4a) and slip (4b) case.

Normalized vorticity magnitude contours for the no-slip and slip wall cases at x/D = 0 are shown in Figures 4a and 4b. As expected the walls are a source of vorticity both inside and outside the hole for the no-slip boundary condition case. For the no-slip case, the vorticity levels inside the hole that correspond to the counter-rotating vortices are small compared to the vorticity generated in the boundary layer. For both cases, vorticity is also generated by the jet-mainstream interaction, and can be seen from the high contour levels at the jet-mainstream interface. There are two major differences for the slip wall case. First, there is no vorticity inside the hole. Second, the peak vorticity levels are higher, with the exception of the boundary layer, due to a more intense jet-mainstream interaction. The latter is due to the absence of boundary layers to reduce the velocity gradients. This can be seen clearly in Figures 5a and 5b, which compare the velocity contours for the two cases. The velocity contours indicate a much stronger shear layer between the jet and the mainstream for the slip wall case, which is consistent with the higher vorticity levels.

Similar results at x/D = 1, are shown in Figures 6a, 6b, 7a and 7b. From the velocity vectors in Figure 6a and 6b, it is clear that the counter-rotating vortices exist for both cases. Figure 6c shows secondary velocity vectors as measured by Pietrzyk (1989). Note that Pietrzyk's data indicates an x/D of 2. In Pietzryk's work, x-dimension measurements were taken from the upstream side of the hole; therefore, an x/D of 2 in Figure 6c corresponds to an x/D of 0.875 in the present study. Figure 6c can be compared to the predictions in Figure 6a. Good agreement can be

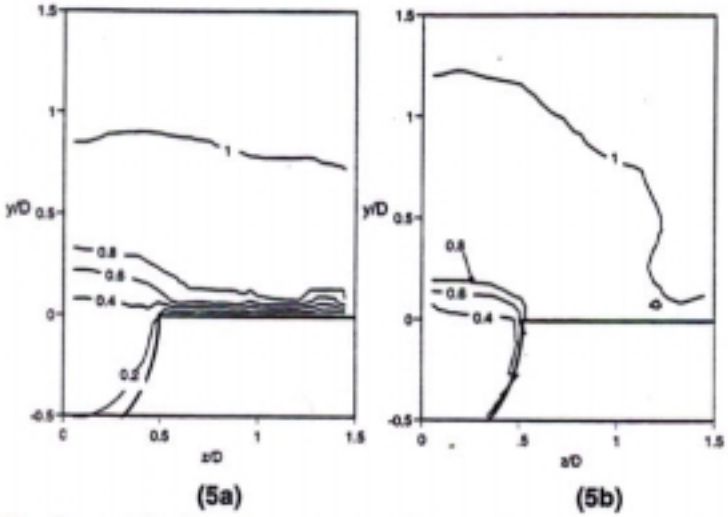

Fig. 5a and 5b Contours of normalized velocity magnitude (V/U_∞) at x/D = 0 for no-slip (5a) and slip (5b) cases.

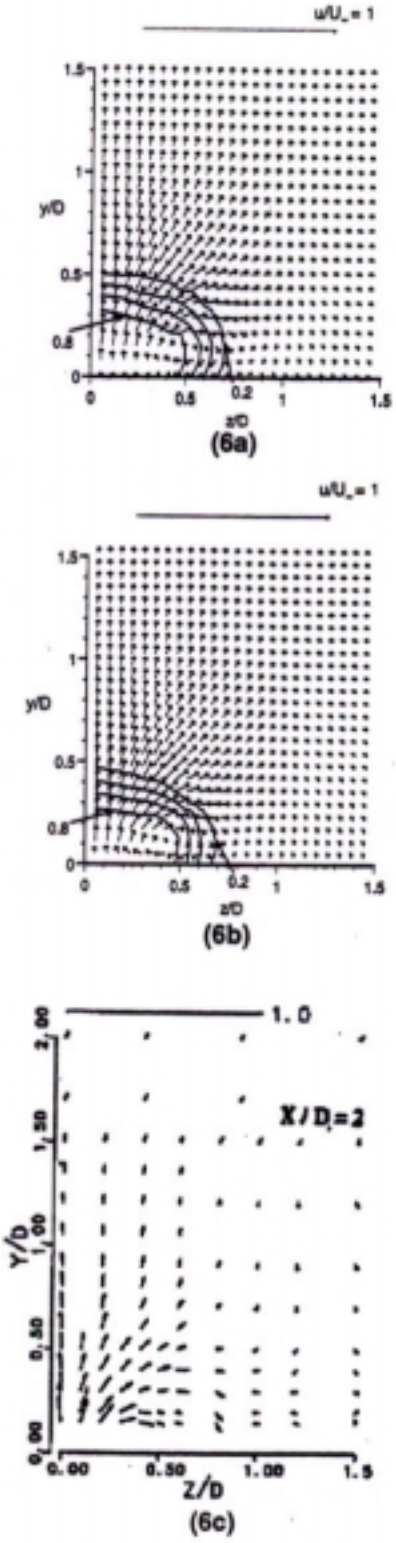

Fig. 6a,6b and 6c Non-dimensional velocity vectors and thermal field contours (θ) at x/D = 1 for the no-slip (6a) and slip (6b) cases, as well as Pietrzyk data (1989) (6c).

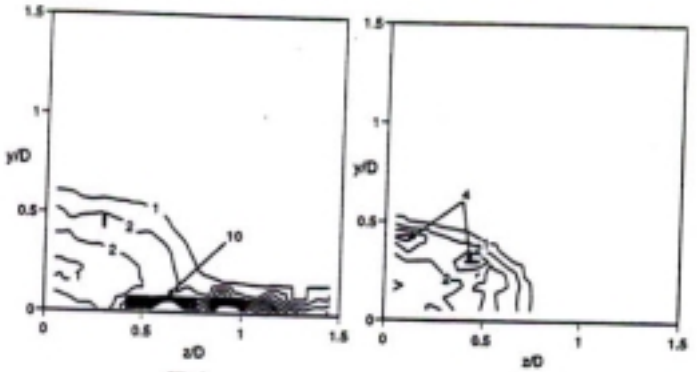

Fig. 7a and 7b Contours of normalized vorticity magnitude (Ω^*) at x/D = 1 for the no-slip (7a) and slip (7b) cases.

seen between these two figures; the locations of the vortex centers are very similar. These results suggest that the vorticity and the counter-rotating vortex inside the film-cooling hole do not form the counter-rotating vortices downstream of the hole exit. Instead,the formation of this counter-rotating vortex pair is governed by the shear layer interaction between the jet and mainstream. This is consistent with the stronger vortex motion for the slip wall case. The vorticity contours at x/D = 1, shown in Figures 7a and 7b, are consistent with the above results. The peak vorticity value for the slip wall is $\Omega^* = 4$ compared to $\Omega^* = 2$ for the no-slip wall (disregarding the boundary layer vorticity levels).

The same trends can be seen in the results further downstream, at x/D = 5, as shown in Figures 8a, 8b, 9a, and 9b. The velocity vectors indicate that the counter-rotating vortex is getting weaker for both cases. Mixing due to the shear layer upstream and the counter-rotating vortex itself have diluted the thermal field and the thermal field contours look much the same for the two cases. Once again, the vorticity magnitude contours shown in Figures 9a and 9b for the no-slip and slip conditions at x/D = 5 indicate similar patterns, but with higher levels occurring for the slip condition.

The vortex center for the slip wall is closer to the wall and jet centerline compared to the no-slip wall case. This is illustrated in Figure 10, which tracks the center of the counter-rotating vortex as it moves downstream of the hole exit. As the jet moves further downstream, the

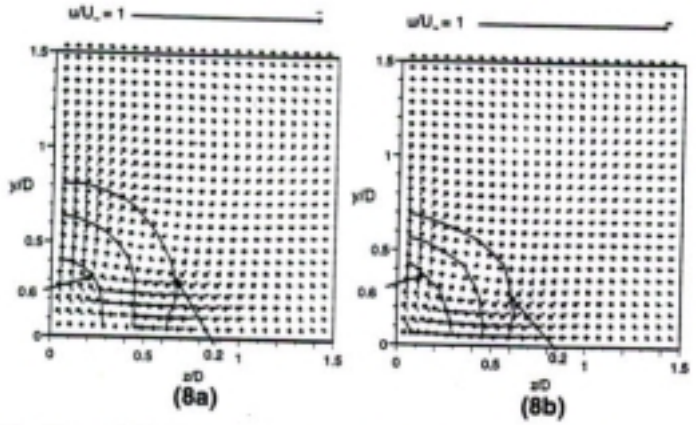

Fig. 8a and 8b Non-dimensional velocity vectors and thermal field contours (θ) at x/D = 5 for the no-slip (8a) and slip (8b) cases.

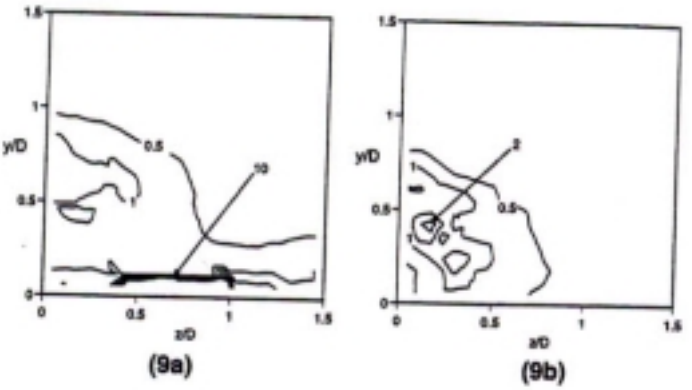

Fig. 9a and 9b Contours of normalized vorticity magnitude (Ω^*) at x/D = 5 for the no-slip (9a) and slip (9b) cases.

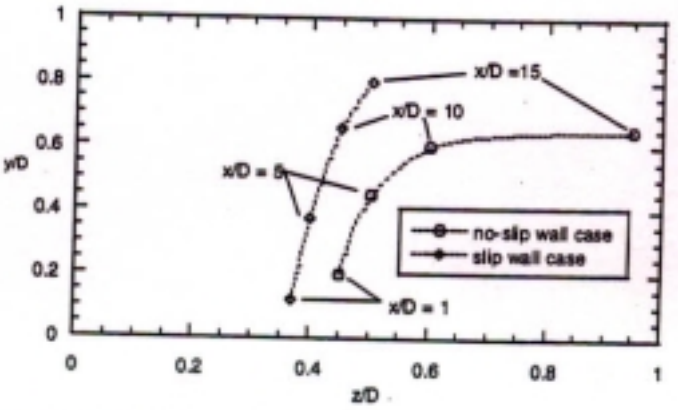

Fig. 10 Center of counter-rotating vortex as it moves downstream for both no-slip and slip wall cases.

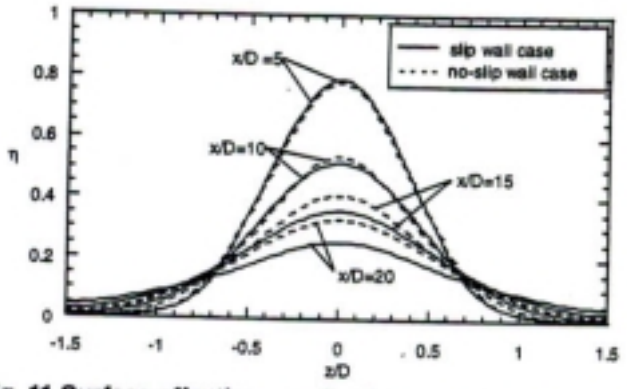

Fig. 11 Surface effectiveness for the no-slip and slip cases.

paths diverge further. As the vortex pair is stronger and closer together for the slip wall case, the two counter-rotating vortex cores pentrate further into the mainstream. Due to the vortices being located further from the wall, the jet mixes with hotter mainstream fluid, causing a more rapid diffusion of the jet.

Conclusions

Results from this study indicate that the formation of the counter-rotating vortices is dictated by the shear layer between the cooling jet and mainstream. The counter-rotating vortices were shown to form in the absence of boundary layers and vorticity inside the cooling hole. These conclusions were possible because of a numerical analysis where slip walls were used to remove boundary layers and vorticity inside the hole. This allowed us to isolate the effect of the jet-mainstream interaction.

The vorticity in the hole region was shown to correlate with the velocity gradients at the jet-mainstream interface. With a stronger shear layer, the slip wall results showed higher vorticity levels than the no-slip wall.Counter-rotating vortices are detrimental to the cooling effectiveness of film-cooling jets. Based on the results of this study, any efforts to minimize the effect or strength of these vortices should focus towards reducing the strength of the shear layer between the jet and the mainstream. This shear layer has been identified as being the key mechanism in the formation of counter-rotating vortices.

Acknowledgements

The authors would like to thank the National Science Foundation for supporting this work through the CAREER award.

References

Andreopoulos, J. and Rodi, W. ,1984, "Experimental Investigation of Jets in a Crossflow," *Journal of Fluid Mechanics*, Vol. 138, pp. 93-127.

Bogard, D.G., 1998, Personal Communication.

Berhe, M. K. and Patankar, V. ,1996, "A Numerical Study of Discrete-Hole Film Cooling," ASME Paper No. 96-WA/HT-8.

Coelho, S.L.V. and Hunt, J. C. R. ,1989, "The Dynamics of the Near Field of Strong Jets in Crossflows," *Journal of Fluid Mechanics*, Vol. 200, pp. 95-20.

Haven, B. A., Yamagata, D. K., Kurosaka, M., Yamawaki, S., and Maya, T. ,1997, "Anti-Kidney Pair of Vortices in Shaped Holes and Their Influence on Film Cooling Effectiveness," ASME Paper No. 97-GT-45.

Kim, S. and Choudhury, D. ,1995, "A Near-Wall Treatment Using Wall Functions Sensitized to Pressure Gradient," ASME Fluids Engineering Div. Summer Conference, Hilton Head, South Carolina.

Kohli, A. and Thole, K. A. ,1997, "A CFD Investigation on the Effect of Entrance Flow Conditions in Discrete Film Cooling Holes," ASME Proceedings of the 32nd National Heat Transfer Conference Vol. 12, pp 223-232.

Launder, B. E. and Spalding, D. B. ,1974, "The Numerical Computation of Turbulent Flows," *Computer Methods in Applied Mechanics and Engineering*, Vol. 3, pp. 269-289.

Leylek, J. H. and Zerkle, R. D. ,1994, "Discrete-Jet Film Cooling: A Comparison of Computational Results with Experiments," *ASME Journal of Turbomachinery*, Vol. 116, pp. 358-368.

Pietrzyk, J. R. ,1989, "Experimental Study of the Interaction of Dense Jets with a Crossflow for Gas Turbine Applications," Ph. D. Dissertation, University of Texas at Austin.

Pietrzyk, J. R., Bogard, D. G., and Crawford, M. E. ,1989, "Hydrodynamic Measurements of Jets in Crossflow for Gas Turbine Film Cooling Application," *ASME Journal of Turbomachinery*, Vol. 111, pp. 1139-145.

Sgarzi, O. and Leboeuf, F. ,1997, "Analysis of Vortices in Three-Dimensional Jets Introduced in a Cross-flow Boundary Layer," ASME Paper No. 97-GT-517.

Vogel, D. T. ,1998, "Numerical Investigation of the Influence of Specific Vortex Generation on the Mixing Process of Film Cooling Jets," ASME Paper No. 98-GT-210.

Walters, D. K. and Leylek, J. H. ,1997, "A Detailed Analysis of Film-Cooling Physics Part I: Streamwise Injection with Cylindrical Holes," ASME Paper No. 97-GT-269.